Do you BET on routine? The reliability of N2 physisorption for the quantitative assessment of biochar's surface area

Do you BET on routine? The reliability of N_2 physisorption for the quantitative assessment of biochar's surface area

Przemyslaw Maziarka[X1], Christian Wurzer*[X2], Pablo J. Arauzo[3], Alba Dieguez-Alonso[4], Ondřej Mašek[2], Frederik Ronsse[1]

[1] Department of Green Chemistry and Technology, Faculty of Bioscience Engineering, Ghent University, Coupure Links 653, 9000 Gent, Belgium

[2] UK Biochar Research Centre, School of GeoSciences, University of Edinburgh, Alexander Crum Brown Road, Edinburgh, EH7 3FF, United Kingdom.

[3] Department of Conversion Technologies of Biobased Resources, Institute of Agricultural Engineering, University of Hohenheim, Garbenstrasse 9, DE-70599 Stuttgart, Germany

[4] Institute of Fluid Dynamics and Thermodynamics, Faculty of Process and Systems Engineering, Otto-von-Guericke Universität Magdeburg, Universitätsplatz 2, DE-39106 Magdeburg, Germany

[X] These authors share first authorship and contributed equally to the work

Abstract

A large specific surface area is one of the structural characteristics which makes biochar a promising material for novel applications in agriculture and environmental management. However, the high complexity and heterogeneity of biochar's physical and chemical structure can render routine surface area measurements unreliable. In this study, N_2 and CO_2 characterization of twelve biochars from three feedstocks with production temperatures ranging from 400 °C to 900 °C were used to evaluate materials with varying structural properties. The

* Corresponding author. Tel: +44 747 3621 354. E-mail: c.wurzer@ed.ac.uk (Christian Wurzer)

results indicate that the frequently reported peak in the surface area of biochars around 650 °C is an artefact of N_2 measurements and not confirmed by CO_2 analysis. Contradicting results indicate an influence of the structural rigidity of biochar on N_2 measurements due to pore deformation in certain biochars. Pore non-specific calculation models like the Brunauer-Emmett-Teller method do not allow for adjustments to these changes. Instead, the use of a pore specific model and the exclusion of pores smaller than 1.47 nm was found to achieve more representative results. The proposed calculation was validated on an external dataset to highlight the applicability of the method. Our results provide novel insights for understanding the structural evolution of biochar related to production temperature.

Keywords

Engineering biochar, biomass pyrolysis, pore size distribution, specific surface area, pore volume

1. Introduction

In the face of climate change, biochar has received an increasing interest as a novel class of materials suitable for long term carbon sequestration as recently recognized by the IPCC [1]. Biochar, the solid product of biomass pyrolysis, can be produced from a wide variety of feedstocks and by a range of production techniques [2]. The properties of the material are shaped by both the pyrolysis conditions, e.g. the highest treatment temperature (HTT), and feedstock parameters such as the lignocellulosic composition or ash content [3]. Due to these various possibilities of feedstock and production parameter combinations, biochars constitute a versatile class of materials with multifunctional properties [4]. Research on biochar application comprises, among other things, the use as a soil amendment [5, 6], in gas and water filtration [7], in metallurgy [8], or as electrode material for batteries and supercapacitors [9, 10]. These

different uses require biochar to possess application-specific properties to be efficient. The concept of engineered biochar aims at producing biochar with predefined characteristics by identifying fitting production parameters and feedstocks [11, 12]. Therefore, knowledge about the interplay between biomass characteristics, conversion mechanisms and resulting biochar properties is the basis for tailoring biochar to certain applications. Temperature series of biochars produced at varying HTTs are conducive to study the effects of specific parameters and enable general conclusions about the underlying mechanisms [11, 13, 14]. However, biochars produced at different HTTs exhibit large differences in their structural form and chemical properties and characterization techniques need to be unbiased towards these changes to enable reliable comparisons [3, 15]. As biochar research is still an evolving field, characterization techniques from established research areas such as soil science or related materials like activated carbon are often used to characterize biochar [16, 17]. Nonetheless, as a complex class of materials, the diverse properties can present specific challenges, which might render established characterization techniques unreliable when applied to biochar [18, 19].

The structural rearrangement of biomass with increasing HTT is one of the determining factors for predicting the final product properties. While molecular models on the structural reorganization have been proposed [20-22], less is known about derived characteristics such as the evolution of surface area (SSA), pore volume (V_{pore}), and pore size distribution (PSD), impeding accurate pre-pyrolysis predictions of these parameters as required for engineering biochar. The importance of the SSA stems from the fact that it determines the number of potential interaction sites with the surrounding matrix. At the same time, the pore size distribution allows conclusions about their physical accessibility, with both carrying significant implications for the final performance of the material [23-25]. Emerging applications for biochar such as gas and water filtration often require large surface areas and pore volumes within specific pore size ranges to be efficient. While narrow micropores are a prerequisite for

efficient CO_2 separation [26], larger micropores are required for the use as an electrode material [27], and a mixed pore size range for the filtration of pharmaceuticals from wastewater [28]. Biochar engineering therefore dependents on an accurate characterisation of these parameters to get an understanding of pore development mechanisms, which can then be utilised for the design of biochars with pre-defined properties.

Conventional methods for assessing the SSA, $V_{pore,}$ and PSD are based on low-temperature gas physisorption. Although general trends have been observed, such as a rise and fall of SSA with increasing HTT, these are empirically drawn from a limited set of measurement methods and often lack detailed theoretical validation or cross-examination with other techniques [12, 29]. Especially the evolution of SSA and PSD with HTT and feedstock composition remains inconclusive [12]. While N_2 (at 77 K) is the most common probe molecule for the determination of the SSA, alternative adsorbates such as CO_2 (at 273 K), Ar (at 77 or 87 K) or Kr (at 77K) might also be used, with specific advantages and disadvantages for each method [30-33]. However, to date, these are seldomly applied for the characterization of biochar. Irrespectively of the type of probe molecule, the calculation of derived parameters such as the SSA is based on an experimental isotherm. Prior to the isotherm measurement, sample preparation requires a degassing step (e.g., under vacuum or He gas atmosphere) and elevated temperature to remove adsorbed matter. As shown by Sigmund et al. [18], biochar already presents significant complications at the degassing stage as structural changes might occur with the application of standard degassing protocols derived from related materials, i.e. activated carbon carbon black. The measurement of the experimental isotherm itself proves similarly challenging, especially with the commonly used N_2. The complex pore structure and low measurement temperature (77 K) can lead to prolonged equilibrium times of up to several days due to diffusion limitations [34]. Correct parameter settings such as the choice of an appropriate equilibrium time are therefore especially important as non-equilibrium conditions can lead to varying results [32-

35]. Another specific characteristic of N_2 isotherms of biochar is open hysteresis, which is incompatible with standard IUPAC classifications or calculation models [30]. Open hysteresis is often simplified as a result of non-equilibrium conditions and mostly ignored in biochar characterization even though its occurrence might be related to structural characteristics of biochars. However, in studies on carbon capture and storage, structural deformation receives greater interest as it can be associated with the adsorbent's performance [36-38]. Pore deformation induced by low-pressure N_2 adsorption is the result of elevated localized pressure during the filling of narrow micropores. This adsorption induced stress causes the expansion or contraction of pores if the adsorbent structure is non-rigid. So far, adsorption induced pore swelling has been observed for fossil coal, activated and synthetic carbons, and metal-organic frameworks [39-42]. However, as observed by Braida et al. [43], benzene sorption can provoke swelling in biochar, demonstrating a similar non-rigidity of biochar's carbon structure. Therefore, it is plausible that N_2 adsorption induced swelling might occur as well.

Once the experimental isotherm is determined, a variety of models exist to calculate derived quantitative parameters such as SSA, V_{pore} or PSD. These models can be further divided into pore-specific and pore non-specific methods, which differ in their ability to differentiate between pore sizes and are well described in the literature [32, 33]. The almost universally used pore non-specific method to calculate the surface area from N_2 isotherms is based on the theory proposed by Brunauer-Emmett-Teller (BET), which is also recommended by the European Biochar Certificate (EBC) [44]. Although widely used, the BET method was initially developed for nonporous materials with a uniform surface and is conceptually weak for heterogeneous materials, i.e. biochar [45]. One of the few parameters relevant for the correct application of the BET theory is the applied p/p_0 range, with the original method suggesting a standard p/p_0 range between 0.05 and 0.35, typically reduced to 0.1 and 0.3 in biochar research [32, 33, 46]. Although this range proves to be appropriate for the original purpose, it is only valid in the

absence of microporosity or strongly adsorbing sites. In the presence of micropores, the valid p/p_0 range should be identified by applying additional selection criteria as specified by Rouquerol et al. [47]. To determine if the p/p_0 selection is appropriate, the calculated C parameter, which describes the energy of monolayer adsorption, can then be utilized [35]. As the C parameter has to be of positive value, a negative C parameter explicitly indicates a wrong p/p_0 range selection and in consequence an invalid result. Despite semi-automated BET-assistants in modern instruments which suggest a valid p/p_0 range, the often inappropriate use of the standard range can still be found in the published literature [48]. Because of these shortcomings, in practical terms as well as in the theoretical assumptions of the BET theory, the comparability of $SSA_{(BET)}$ values for biochar is highly variable. Pore specific techniques based on the Density Functional Theory (DFT) or Grand Canonical Monte Carlo simulations (GCMC) are advanced computational methods overcome the main obstacles of pore non-specific models by simulating the adsorption of fluids on a molecular level [49]. For biochars displaying semi-continuous pore size distributions in the micro and mesopore size range, the DFT approach avoids the erroneous averaging approach shown by pore non-specific methods like BET [32, 33, 35]. Especially promising for the analysis of biochars are recently developed kernels for N_2 adsorption on carbons with complex surface structure such as the Heterogeneous Surface Non-Local DFT (HS-NLDFT, Micromeritics) or Quenched Solid DFT (QSDFT, Quantachrome), which despite differences in the calculation procedures, show generally comparable results [50].

Similar to classical approaches such as the BET method, DFT models will be significantly affected by errors in the isotherm measurement. However, no detailed studies on the effects of physisorption parameters on N_2 isotherms of biochar exist today. Due to a lack of standardization and incomplete reporting of experimental parameters, the influence of measurement conditions on the results is difficult to identify as shown by Bachmann et al. [51].

One way to cross-validate the assessment of N_2 isotherms on microporous carbonaceous materials is the use of CO_2 as a complementary analysis in the overlapping pore size range between 0.7 nm and 1.47 nm [52]. The upper range of pore size determination of approximately 1.47 nm for standard instruments limits the sole use of CO_2, but the overlapping range between 0.7 nm and 1.47 nm can be used to assess the reliability of the N_2 isotherm. Due to the slow diffusion of N_2 at 77 K, especially in narrow micropores of biochar and related inconsistencies, Jaggiello et al. [61] proposed a lower p/p_0 limit for N_2 measurements of 10^{-3} to avoid non-equilibrated measurements. The analysis is complemented with CO_2 measurements of the narrow micropore range. While the combination of N_2 and CO_2 has several advantages and must be seen as a benchmark method for biochar characterization, it is seldomly used in literature to date.

Surface area measurements should ultimately provide a reliable assessment of biochar properties and ensure comparability between samples. In this study, we analyzed the temperature series of biochar produced from three different feedstocks by pyrolysis at 400 °C, 500 °C, 700 °C, and 900 °C. Physisorption measurements using N_2 and CO_2 as probe molecules allow a comprehensive analysis of the micro and mesopore range. We calculated the surface area of the samples from N_2 isotherms by the traditional BET method as well as more advanced DFT models to allow a comparison of pore specific and pore non-specific methods. Based on the results of pore size distributions calculated from N_2 and CO_2 measurements in the overlapping pore size range from approximately 0.7 nm to 1.47 nm, we propose an adjusted DFT calculation as a more reliable method for the assessment of biochars. To ensure the applicability of our analysis and to avoid any bias introduced within our experiments, we obtained external data from published literature to test the general applicability of our proposed method.

2. Materials and methods

2.1 Biochar production

In this study, rice husk (RH) and wheat straw (WS) biochars were produced from the UKBRC Standard biochar feedstocks [53]. The feedstocks were first shredded and sieved to obtain particles in size range from 0.5 mm to 1 mm. Pyrolysis was conducted in a thermogravimetric analyzer (TGA/DSC 1 - Mettler Toledo, CH) by placing approximately 100 mg of each sample in an alumina crucible. The sample was heated in a N_2 atmosphere (50 ml/min) at 10 °C/min to 110 °C and held for 10 min to remove residual moisture. Then, the sample was heated at 20 °C/min to the HTT of 400 °C, 500 °C, 700 °C, or 900 °C with a residence time of 10 min. Consequently, the sample was cooled down in N_2 atmosphere to room temperature before removal from the furnace. All samples were pyrolyzed at least in 20 replicates to obtain sufficient sample for subsequent physisorption experiments. All samples were finely ground in an agate mortar prior to characterization.

Beech wood cylinders (Ø8x16 mm) obtained from Rundstäb (Meyer & Weigand GmbH, Nördlingen, Germany) were used for the production of wood biochar (WD). The feedstock was dried overnight at 105 °C prior to pyrolysis. Each sample was pyrolyzed individually in a Single Particle Reactor (Best-Research GmbH, Graz, Austria). Pyrolysis runs were conducted in 6 repetitions, at 4 different temperatures: 400 °C, 500 °C, 700 °C with a residence time of 10 min at HTT, and 900 °C with a residence time of 5 min. Afterwards, the samples were finely ground in an agate mortar prior to characterization.

All samples in this study were labelled according to their feedstock (RH, WS, WD) followed by the highest treatment temperature in °C (HTT), i.e. rice husk biochar produced at 400 °C is named RH400.

2.2 External data set

For the assessment of a wider variety of feedstocks and production conditions, N_2 and CO_2 isotherm data from published literature was obtained by requesting raw data from the corresponding authors. Articles were selected based on the criteria of reporting data on non-amended biochar produced by slow pyrolysis and focused on recently published articles. For CO_2 data, there was no limitation regarding the publication date as only a few potential articles could be identified. 53 inquiries were made, from which 9 authors submitted raw data comprising 50 (N_2) and 11 (CO_2) records. A sample list including the used feedstocks and original publications can be found in the supplementary information (SI).

2.3 Physisorption measurements

Around 200 mg of each sample was degassed at 180 °C for 24 h to remove residual moisture and volatiles prior to the measurements. The adsorption of N_2 was measured at 77 K in the p/p_0 (N_2) range between 10^{-3} and 0.995 with 40 adsorption and 30 desorption points. Measurements were done on a Nova 4000e analyzer (Quantachrome Instruments) operated in standard mode (target pressure mode - TP). TP uses repetitive dose injections until equilibrium at a prespecified target pressure point is achieved. Equilibrium time was set to 3 minutes, after which a pressure point was accepted if adsorption did not change for more than 0.001% of the adsorbed volume. Samples analyzed in Constant Volume (CV) mode (VectorDose^{TM}) were analyzed on an Autosorb-iQ (Quantachrome Instruments). In CV mode, the injected dose volume is specified beforehand, and an isotherm point is locked if equilibrium conditions are achieved. Equilibrium time was also set to 3 minutes. Physisorption measurements using CO_2 as adsorbate were conducted at 273 K on a Nova 4000e analyzer (Quantachrome Instruments) with sample pre-treatment similar to N_2 measurements. CO_2 measurements were performed in the relative pressure range between 10^{-4} and $3 \cdot 10^{-2}$ p/p_0 (CO_2) with 30 adsorption and 13 desorption points in target pressure mode.

2.4 Isotherm analysis

Experimental isotherms were analysed using Quantachrome's NovaWin and ASiQWin software as well as SAEIUS software (Micromeritics). As a pore non-specific method, the SSA was calculated using the BET method ($SSA_{(BET)}$) in the standard pressure range as initially proposed by Brunauer et al. [46] and in the adjusted pressure range, according to Rouquerol et al. [47]. Pore specific analyses were done on the adsorption branch of the isotherms, according to recommendations for open hysteresis isotherms [32]. As a pore specific method, the Heterogeneous Surface Non-Local Density Functional Theory (HS-NLDFT) with a minimum pore width of 0.7 nm was used. The surface roughness factor Lambda was selected between 1.5 and 2.5, based on the L-curve method. The DFT models were calculated on the whole range p/p_0 (N_2) which corresponds to a pore size range between 0.7 nm and 30 nm. Quenched Solid Density Function Theory (QSDFT) on carbon assuming slit/cylindrical pores was used as a complementary DFT model. External data sets were analyzed similar to the experimental data produced for this study, but only the HS-NLDFT method (SAIEUS software, Micromeritics) could be used due to variable data formats. The CO_2 isotherms were analyzed by GCMC (Grand Canonical Monte Carlo) based on the whole p/p_0 range, which corresponds to pore sizes between 0.35 nm and 1.47 nm.

3. Results and discussion

3.1 N_2 isotherms

The N_2 isotherms for the RH biochars are presented in Figure 1, WD and WS biochars can be found in the SI (Figure S1). The isotherm shapes are similar between biochars produced at the same temperature, although substantial differences in the adsorbed volumes are observed. Moreover, all isotherms exhibit open hysteresis which is characterized by non-closing of the desorption part of the isotherm with the adsorption branch at low p/p_0. The adsorption branch

of the isotherm from samples produced at HTT 400 °C indicates non- or macroporous materials (IUPAC classification: type II) [35]. Monolayer formation is achieved at low p/p_0 as shown by the sharp knee of the isotherm. At 500 °C, WD and RH samples show higher adsorption volumes in the low p/p_0 range than WS500 and relevant adsorption occurring at the lowest measurement point of 10^{-3}. While RH and WS biochars show a steep rise at high p/p_0 ranges, wood biochar proceeds to a plateau shape isotherm.

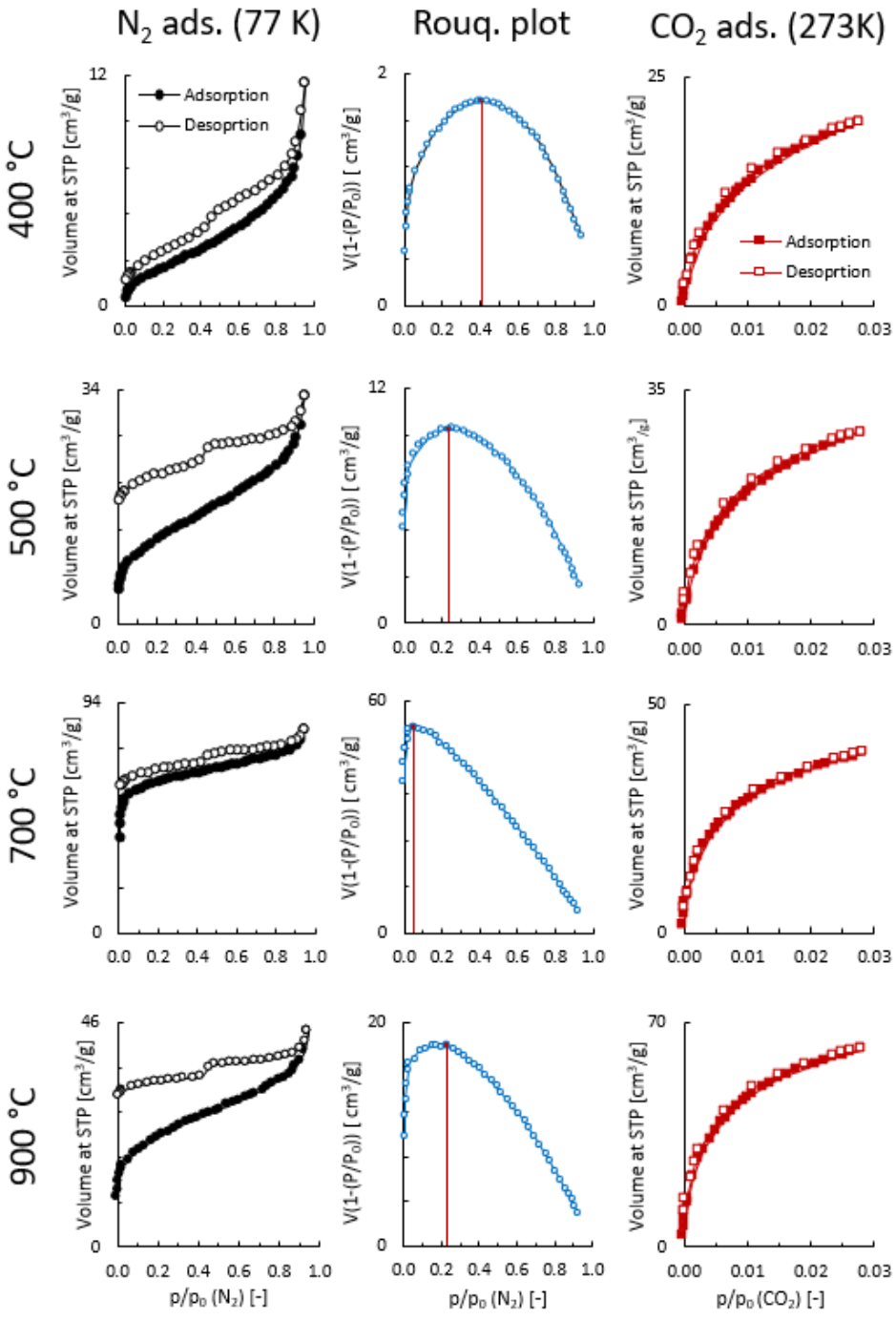

Figure 1: *Evolution of N_2 and CO_2 isotherms with the highest treatment temperature for rice husk biochars. Rouquerol plots indicate the maximum applicable p/p_0 range (N_2) for $SSA_{(BET)}$ calculation (red line).* ***Left*** *- N_2 isotherms,* ***Centre*** *- Rouquerol plots,* ***Right*** *- CO_2 isotherms.*

At a HTT of 700 °C, the shape of RH and WD isotherms indicates strongly microporous materials (IUPAC classification: type I(b)) [35]. A large increase in the maximum adsorbed volume (RH500 33.4 cm^3/g and RH700 82.7 cm^3/g) can be observed, in line with a drastic increase in the adsorption volume at the first measurement point. Contrary to changes in the isotherm shape observed for RH and WD biochars, WS biochar displays no change in the shape of the isotherm or the adsorbed volumes up to HTT of 700 °C (Figure S1). WD and RH samples produced at HTT 900 °C exhibit a significant reduction of the adsorption volume compared to HTT 700 °C as well as reduced adsorption at the first measurement point. Contrary to the other feedstocks, WS900 displayed a shift to higher adsorbed volumes accompanied by relevant adsorption at the first measurement point, indicating increased microporosity.

3.2 Pore non-specific model: BET

According to the BET theory, the assessment of the SSA requires the selection of an applicable p/p_0 range to calculate the C parameter from which the SSA is derived [35]. The standard range for biochar characterisation is often set to 0.1 to 0.3 [32], however microporous materials can reach monolayer coverage already at lower pressures, and the standard range is no longer valid [32, 33, 35, 47]. The C parameter, which is related to the energy of monolayer adsorption, is used to assess the correct pressure range selection. As negative energy of adsorption lacks physical meaning, a negative C parameter constitutes an invalid pressure range selection, e.g. the C parameter of RH700 and RH900 calculated from the standard range (Table 1). Data for WS and WD can be found in Table S1.

Table 1: *Comparison of the BET analysis results from N_2 adsorption using the standard (0.1-0.3) and adjusted p/p_0 range according to Rouquerol's criteria for rice husk biochars. C parameter – BET constant indicating material specific net heat of adsorption; SSA – specific surface area.*

	BET - standard range			BET - adjusted range		
Sample	p/p_0 range [-]	C [-]	SSA [m^2/g]	p/p_0 range [-]	C [-]	SSA [m^2/g]
RH400	0.10-0.30	19	8.4	0.12-0.41	19	8.3
RH500	0.10-0.30	121	43.9	0.06-0.23	74	45
RH700	0.10-0.30	-35	139.3	0.02-0.05	1768	233.4
RH900	0.10-0.30	-186	75.2	0.11-0.17	200	79.7

Rouquerol et al. [47] proposed selection rules to determine the correct p/p_0 range for microporous materials. Figure 1 shows Rouquerol plots for RH biochars produced at increasing HTT with red lines indicating the adjusted upper limit of the applicable pressure range instead of the fixed limit of p/p_0 at 0.3 as set in the standard range (WD and WS in Figure S2). By comparing the upper p/p_0 limits with the N_2 isotherms, a narrowing of the applicable p/p_0 range in the presence of micropores can be noticed. For samples displaying high microporosity such as WD700, the applicable upper limit is even below the lower limit of the standard range of $p/p_0 = 0.1$. The limitation to low-pressure regions dictates that the $SSA_{(BET)}$ will predominantly display micropores, as larger pores are not covered within this p/p_0 range.

In Figure 2 (top), the adjusted C-values are plotted against the upper limit of the applicable p/p_0 range, i.e. the highest p/p_0 point which can be used according to the selection criteria by Rouquerol, and compared to the non-adjusted C-values from the same samples obtained from the standard p/p_0 range [47]. The asymptotic behaviour of the standard C-values highlights the restrained applicability of the BET method for biochars as displayed in the limited number of samples presenting a positive C parameter. Adjustment of the pressure range according to Rouquerol's selection criteria enables all biochar samples to be assessed as

displayed by the tangential behaviour of the C-values towards zero with increasing p/p_0 range. The importance of selecting the correct p/p_0 range is highlighted in Figure 2 (bottom). Significant errors of up to 30% of the SSA can be introduced by using the invalid standard p/p_0 range for microporous materials in contrast to the adjusted range. Noteworthy, a small, negative value of the C parameter (from std. p/p_0 range) indicates a larger error for the calculated $SSA_{(BET)}$ (Figure 2).

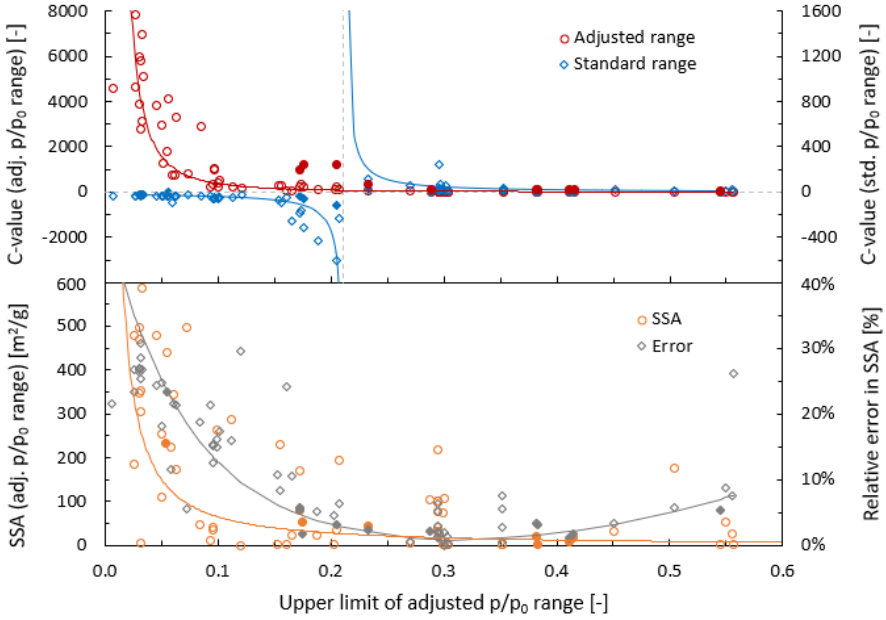

Figure 2: *Influence of the p/p_0 range selection on the C parameter and $SSA_{(BET)}$ values.* ***Top*** *– C parameter values from the adjusted and standard range plotted against the upper limit of the corresponding adjusted p/p_0 range;* ***Bottom*** *– Error of an invalid p/p_0 range selection on the BET value in % of the valid BET value (n =62, filled points – this study, unfilled points – external data [18, 54-62]).*

The exponential increase of C with decreasing p/p_0 limit highlights another general limitation of the BET model for biochars. As the C parameter is related to the energy of adsorption, high values (>150) indicate either the adsorption on high-energy surface sites or micropore filling [35]. Consequently, the assumption of monolayer coverage is questionable and the reliability of the SSA calculation in doubt if the C parameter is high. Within our dataset, a significant number of adjusted C parameters exhibit values above 150 (Table 1, S1 and S5).

Because the BET method is pore non-specific, no further assessment of the influence of micropores on the surface area calculation of biochars is possible based on this method.

3.3 Pore specific model: HS-NLDFT

As a pore specific method, the HS-NLDFT was used to assess V_{pore}, SSA and PSD of the whole dataset, i.e. internal and external data. The observed linear relationships of micropore volume and $SSA_{(BET)}$ are similar to observations from Centeno and Stoeckli [63] for activated carbons (Figure S5). A division of the total surface area and pore volume into micro- and meso-range highlights the dominant role of micropores for samples displaying high C-parameter values. For samples with C > 1000, the surface area of the micropores contributes over 85% to the overall surface area, with a strong correlation between the C parameter value and the micropore ratio for SSA (R^2=0.833) as well as V_{pore} (R^2=0.780) (Figure 3; SI – Table S2, S3, S6).

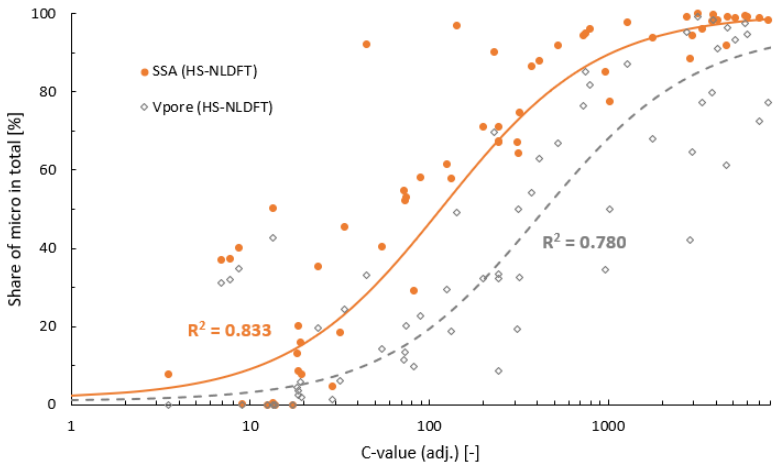

Figure 3: *Proportion of micro-SSA and micro-V_{pore} (HS-NLDFT) from total SSA and pore volume in comparison to C parameter values from the adjusted BET p/p_0 range (n=62, combined dataset from this study and external data [18, 54-62]).*

Pore size distributions (HS-NLDFT) revealed dominant peaks in the micropore region below 1.5 nm as shown for the RH biochars in Figure 4. Similar trends can be seen for WS and WD in Figure S3.

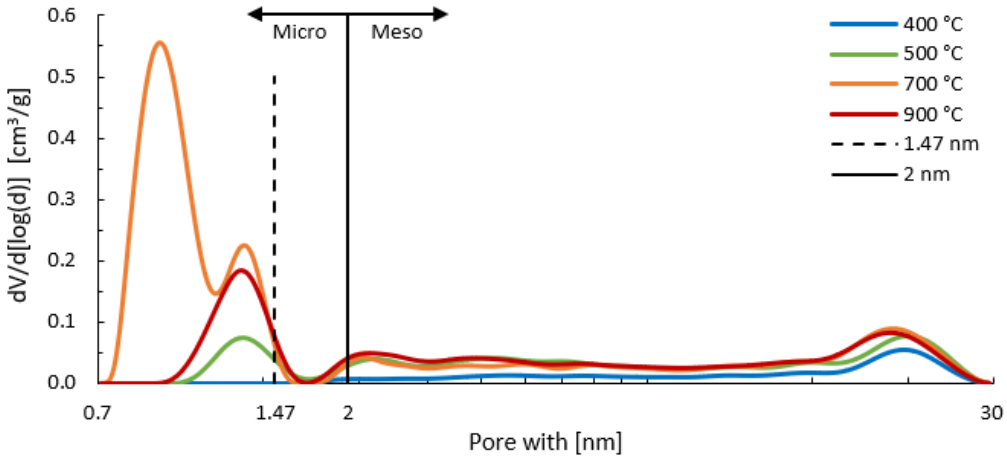

Figure 4: *Pore size distribution (HS-NLDFT) of rice husk biochars from N_2 adsorption (pore size range from 0.7 nm to 30 nm).*

The PSD from biochars of all feedstocks display increasing volumes for pores wider than 1.5 nm with rising HTT but a differing trend in narrow micropores (< 1.5 nm). Most noticeable is the pore volume peak in the narrow pore size region for WD and RH biochars

produced at HTT of 700 °C. While the pore volume of RH biochar expands 4-fold with an increase of HTT from 500 °C to 700 °C, an almost identical decrease with a further rise of the HTT to 900 °C can be observed. Similar trends for a peak in V_{pore} and SSA for biochars produced at a HTT around 700 °C are often seen in literature and commonly explained by a pore structure collapse at higher treatment temperature [12, 60, 64-67]. However, as exemplified by RH biochars in this study, no significant differences in larger micropores or mesopores can be observed, indicating that major structural changes such as pore collapses are unlikely as hypothesized by Brown et al. [67]. Since the dominant peak in the narrow micropore range is solely responsible for the substantial increase in SSA and depends on the initial measurement point (Figure 3), we hypothesize that the measurement itself might be responsible for the apparent SSA peak (Table 1). As the N_2 measurements do not start in close vicinity to zero, adsorption at the lowest p/p_0 point of 10^{-3} represents a cumulative value for pores smaller than the initial isotherm point. Similar disturbances of results are known for the desorption branch of DFT models for activated carbons [68]. Therefore, micropore filling in micropores below 1 nm cannot be ruled out. If micropores are already filled at the initial isotherm point, the N_2 isotherm cannot be used to provide a valid monolayer capacity (BET) nor an accurate pore size distribution (e.g. HS-NLDFT) [35]. It is noteworthy that N_2 measurements of biochars in pressure regions below 10^{-3} are seldomly conducted nor recommended as these require more advanced equipment and present experimental difficulties due to slow diffusion of N_2 into the complex pore structure of biochars as observed by Braida et al. [43] and Jagiello et al. [34]. However, elevated p/p_0 ranges for N_2 characterization might obfuscate a valid determination of micropores in biochar, which is problematic due to the dominant influence of micropores on the SSA and V_{pore} (Figure 3). To accurately determine narrow micropores in the pore size range 0.4 nm to 1.5 nm, adsorption of CO_2 at 273 K is recommended due to faster diffusion into narrow micropores [33, 52].

3.4 CO_2 isotherms

In contrast to N_2 measurements, CO_2 adsorption volumes increase steadily with increasing HTT for all feedstocks (Figure S4). The comparison of different feedstocks shows the largest adsorption volumes for WD biochars with WS displaying the lowest ones. However, these differences are of the same magnitude across all samples. Relevant open hysteresis was not observed. Most noticeable, V_{pore} and SSA measured by CO_2 do not show a peak for samples produced at HTT 700 °C as seen in N_2 measurements. Comparing the differential pore volumes (N_2 - HS-NLDFT; CO_2 - GCMC) in the overlapping pore size range between 0.7 nm and 1.47 nm, significant differences between biochars from the same feedstock and between different feedstocks can be observed (Figure 5).

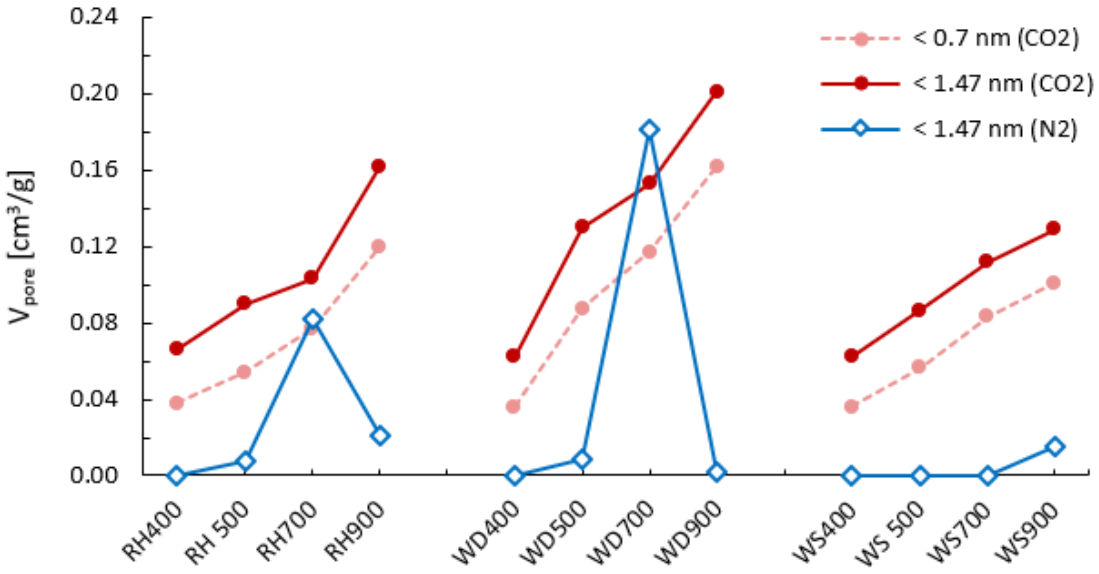

Figure 5: *Comparison of cumulative V_{pore} at different pore widths obtained via adsorption of N_2 (HS-NLDFT) and CO_2 (GCMC).*

In the case of RH and WD biochars produced at 400 °C, 500 °C and 900 °C the micropore volume below 1.47 nm assessed by N_2 is a relatively constant fraction of the corresponding volume measured with CO_2. A larger CO_2 volume can be expected as N_2 adsorption in narrow micropores smaller than 0.7 nm is severely restricted by diffusion

limitations in comparison to CO_2. However, for RH700 and WD700, the ratio between adsorbed N_2 and CO_2 displays a different behaviour. Here the measured volumes by N_2 are almost identical, although a large proportion of the pore volume measured by CO_2 is assessed in the pore range below 0.7 nm (Table S3 and S4). Interestingly, the pore volume calculated from N_2 adsorption exceeds the volume potentially available in this pressure range according to CO_2 adsorption, which was also observed in other studies (Figure S6) [69]. WS biochars present a different pattern than the other two feedstocks. Even though the CO_2 adsorption displays relevant micropore volume, up to 700 °C, no significant N_2 adsorption was detected. Only WS900 exhibits noticeable N_2 adsorption in the narrow micropore range, while CO_2 adsorption followed similar trends as for the other feedstocks. The results from CO_2 adsorption for RH and WD biochars are contradicting the observed N_2 peaks for samples produced at HTT 700 °C. The consistently increasing CO_2 pore volumes with increasing HTT also contradict the assumed micropore structure collapse around 700 °C. By comparing the PSD obtained from CO_2 and N_2 isotherms for RH biochars, the increased adsorption of N_2 in the initial adsorption range for RH700 in comparison to RH900 is clearly visible (Figure 6). Moreover, an even larger difference can be observed in wood-derived biochars (Figure S3).

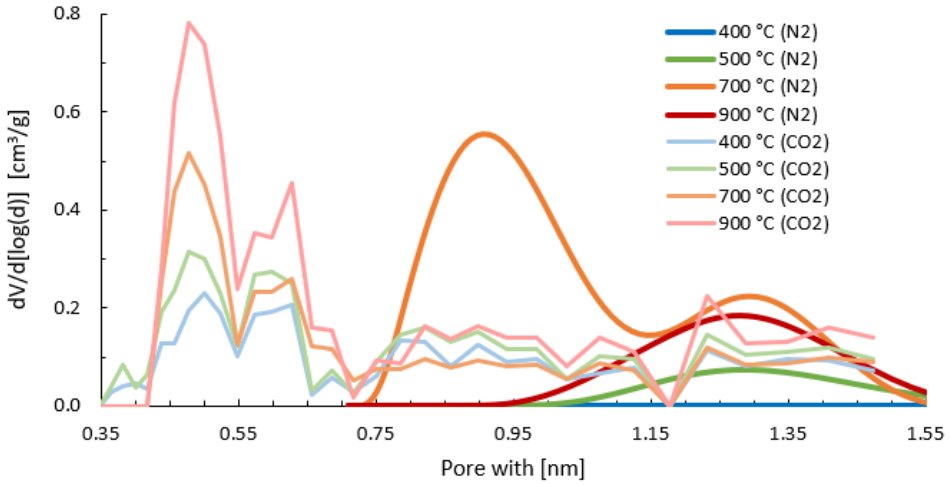

Figure 6: *Comparison of rice husk biochar's PSD in the microporous range derived from N_2 (HS-NLDFT) and CO_2 (GCMC) adsorption (Note: the HS-NLDFT model applies a smoothed PSD model in comparison to the GCMC).*

The monotonical increase in micropore volumes and the corresponding change of PSDs seems more representative for micropore formation with increasing HTT and favours the use of CO_2 in comparison to N_2. A further indication for difficulties in N_2 measurements can be found in the open hysteresis present in most samples, while no relevant hysteresis was observed in CO_2 measurements (Figure 1). While open hysteresis in N_2 measurements of biochar is regularly observed, its origin is not fully understood yet. For related materials such as activated carbon or coal, structural deformation of the carbon matrix during N_2 adsorption is well known and might be an explanation for the observed differences between N_2 and CO_2 measurements.

3.5 The influence of measurement conditions on N_2 adsorption

We hypothesize that if N_2 induced swelling is present, it will be time-dependent and progressing with increasing analysis time at low-pressure regions. To investigate if time is a factor in our measurements, additional measurements on RH700 were conducted applying two methods with differences in the speed of point acquisition but similar equilibrium conditions: constant volume (CV) and target pressure (TP) mode. In TP mode (the standard method) a series of adsorbate doses are injected until a specified target pressure point is achieved. For biochars, this method can lead to several hundred doses and several days to achieve the first measurement point, especially if the target pressure point is set to low pressure, e.g. p/p_0 between 10^{-3} to 10^{-7}. Hypothesizing that swelling is present, elevated acquisition times and dosing will exaggerate the initial adsorption volume. Contrary, the CV mode (e.g. VectorDose^{TM}) injects pre-specified volumes of adsorbate sequentially and uses each dose as a point of the isotherm. Thus, avoiding sequences of smaller doses and sequential equilibrium

periods for individual isotherm points, while still maintaining the same equilibrium conditions, i.e. the specified duration in which no additional adsorbate uptake takes place. Isotherms of the RH700 measurements from both modes and the corresponding PSDs (HS-NLDFT) are shown in Figure 7.

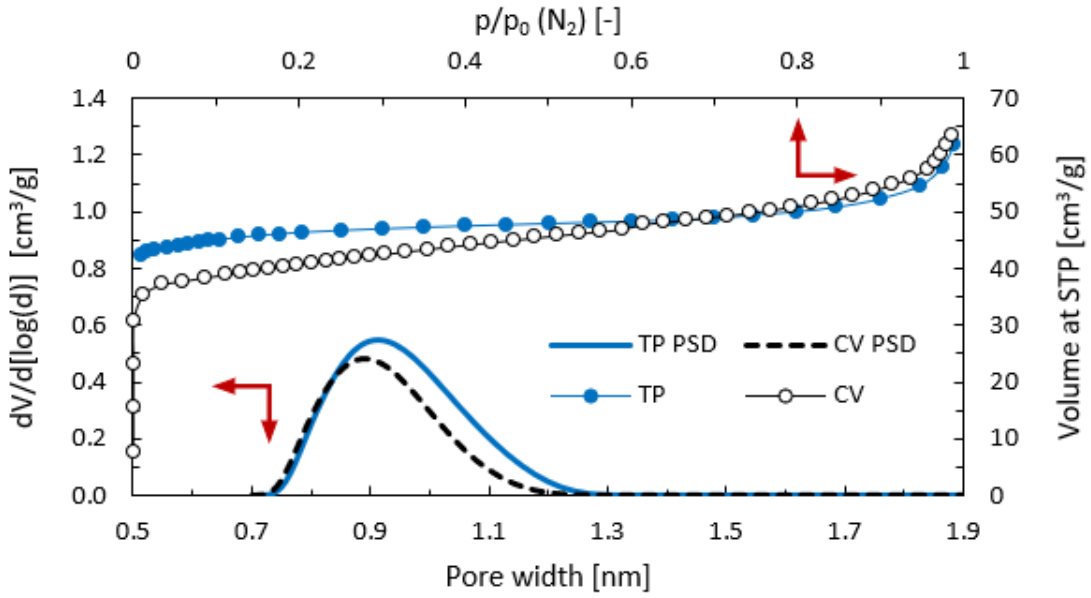

Figure 7: *Comparison of the RH700 isotherms and PSD (HS-NLDFT) from N2 adsorption using different dosing modes (CV – constant volume mode; TP – target pressure mode).*

The acquisition time of the first isotherm point at $p/p_0 = 5 \cdot 10^{-5}$ in CV mode was 33 min. and 831 min analysis time until $p/p_0 = 10^{-2}$ was reached, while 1297 min were required to achieve the first measurement at $p/p_0 = 10^{-2}$ in TP mode. Pore size distributions were calculated on the same p/p_0 range, exhibiting a 20% increase of the cumulative volume at around 1.3 nm in the longer measurement (TP) compared to the CV mode. Additionally, for the CV mode, the PSD peak is shifted to lower pore sizes. A similar pattern for changes in the PSDs caused by swelling was modelled by Hart et al. for microporous polymers [41]. Due to the identical equilibrium conditions of the two measurements, non-equilibrium of the faster analysis is unlikely to be the main factor for the reduced adsorption at low pressures [70]. The differences between the two measurement modes, i.e. the increase of pore volumes in the low-pressure

range with increasing equilibrium time and decreasing p/p_0 range raise further questions about the reliability of N_2 for the measurement of narrow micropores in biochar.

3.6 Open hysteresis and adsorption induced pore deformation

Biochars in this study show open, low-pressure hysteresis in N_2 isotherms as regularly observed in biochar characterisation [33]. In general, open hysteresis in carbonaceous materials is thought to be caused by insufficient parameter selection such as short equilibrium times or experimental issues, like leakage problems [32]. Nevertheless, open hysteresis might also be caused by the material itself through structural deformation of the adsorbent, i.e. swelling, during interaction with the adsorptive [33]. Braida et al. [62] showed that biochars are non-rigid-structured adsorbents during the sorption of benzene and the ability of biochar to swell was further indicated in studies on PAH extraction using organic solvents as well as during H_2O vapour adsorption measurements [71-74].

Deformation of microporous carbonaceous materials during gas adsorption measurements, i.e. swelling or contraction, is related to adsorption induced stress in slit-shaped nanopores embedded in a mobile carbon matrix such as amorphous carbon [39]. During gas adsorption, pores of varying width are exposed to extreme stress in the range of GPa [75, 76]. This local pressure results in pore deformation, i.e. swelling or contraction if the induced stress exceeds the rigidity of the carbon matrix [77, 78]. Balzer et al. [40] simulated positive adsorption stress of 0.2 GPa for a pore size of 0.6 nm at standard N_2 characterization conditions ($p/p_0 = 10^{-3}$, N_2 at 77 K). With the increase of p/p_0 during N_2 adsorption, larger pores up to the mesoporous range become similarly affected although less pronounced. For N_2 adsorption, the induced stress can be neglected only below p/p_0 10^{-9}, while the induced stress by CO_2 at p/p_0 =

10^{-4} is already negligible. Besides the absolute magnitude of induced stress, the direction is of importance and further complicates the identification of stress-induced deformation from N_2 isotherms. Balzer et al. [40] highlighted the oscillating character of adsorption stress between positive (swelling) and negative (contracting) localized stress as a function of the pore size, the relative pressure range and the adsorbate molecule size. Therefore, pores will exhibit a contraction or swelling effect depending on their initial width.

Confirming the lower susceptibility of CO_2 measurement to induce pore deformation, biochars in this study do not display CO_2 hysteresis as opposed to N_2 measurements. For samples with suspected swelling such as RH700 and WD700, the comparison with CO_2 reveals higher differential micropore volumes measured by N_2 which contradict significantly under equilibrium of the isotherms as the adsorbed volumes are higher than expected. It is more likely that N_2 induced swelling of the material is causing elevated adsorption volumes of RH700 and WD700. Additionally, slow diffusion combined with structural deformation could explain the prolonged measurement times, as swelling of the material hinders achieving equilibrium conditions and can lead to artificial peaks in adsorption volumes as seen for other non-rigid materials [52]. This is also indicated by the large differences in analysis time between the two measurement modes for RH700. In TP mode, this dynamic might result in additional iterative dosing and prolongs the analysis to last for several days to achieve equilibrium conditions.

To further isolate the potential effects of structural deformation from non-equilibrium conditions, sequential measurements of CO_2 and N_2 in 3 repetitions were conducted. Sequencing with identical measurement and outgassing conditions enables the identification of structural deformation caused by the measurement itself as non-equilibrium conditions would be similar within the sequence. Sample selection was based on comprising different degrees of suspected swelling, i.e. RH400 < RH900 < RH700. Outgassing was conducted similar to

standard runs between each step. Results from sequential measurements can be found in Figure S7 and S8 in Supplementary Information. For N_2 measurements, the results display no difference for RH400 while higher temperature biochars RH700 and RH900 show relevant divergence in the narrow micropore range. Figure 8 displays the changes in PV for samples RH400, RH700 and RH900 in the affected narrow micropore range.

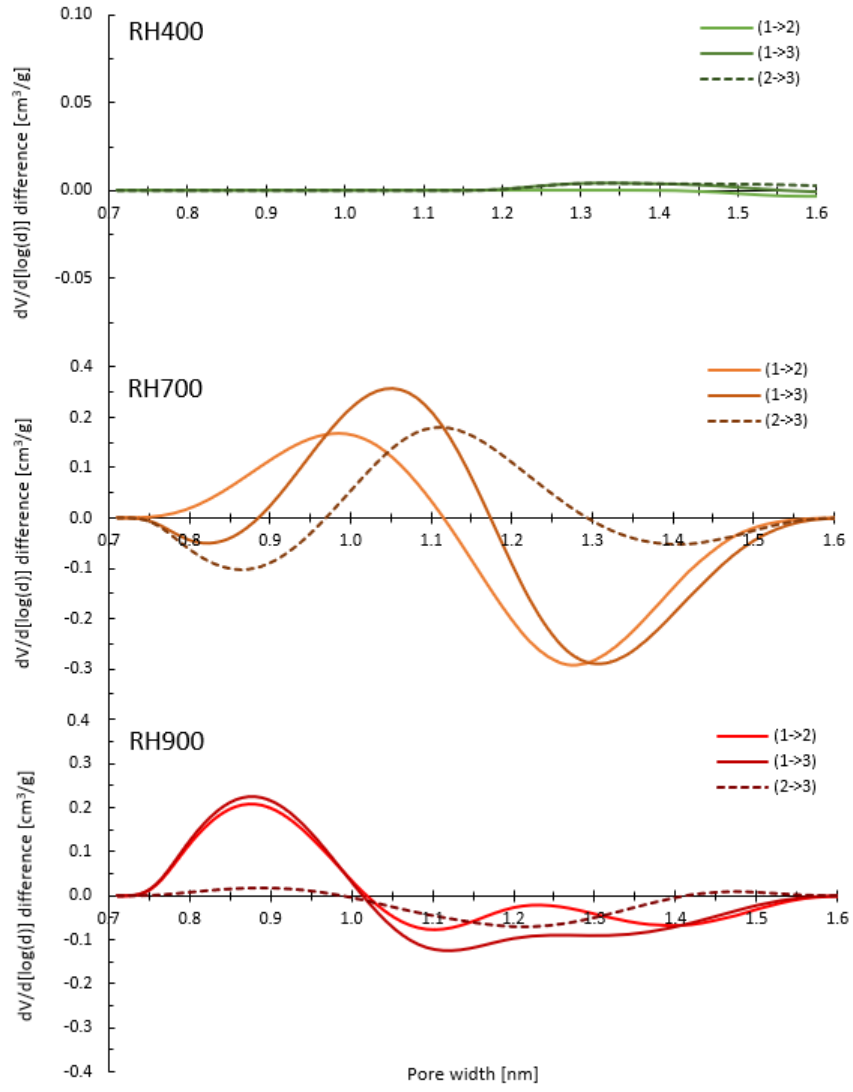

Figure 8: *Differential PSD from N_2 adsorption (HS-NLDFT) between sequential measurements of sample RH400, RH700 and RH900 (1 -> 2 : difference between first and second measurement, etc.).*

A significant increase in differential pore volumes at approximately 1 nm pore width of around 50% was measured for both RH700 and RH900, while larger micropores decreased in volume

for both samples. Sequential CO_2 measurements showed increasing pore volumes in the ultramicropore region < 0.5 nm, but not at larger pore widths (Figure S9). The increase in pore widths at 0.5 nm (CO_2) and around 1 nm (N_2) is accompanied by a decrease in pore volumes between 0.7 nm and 0.9 nm (CO_2), and between 1.2 nm and 1.5 nm (N_2) in subsequent runs. Notably, the increase around 1 nm resembles the difference between the CV and TP measurements mentioned before. The oscillating character of contracting and expanding pore volumes in dependence of pore size matches theoretical modelling of solvation pressures in graphitic slit shape pores made by Diao et al. [79]. Interestingly, RH700 and RH900 show differential peaks at slightly shifted pore sizes. The results indicate the largest divergence occurring in sample RH700, with N_2 measurements being more affected than CO_2 isotherms. This further confirms the susceptibility of the SSA peak for RH700 calculated from N_2 isotherms.

3.7 Influence of structural changes on pore deformation

If adsorption induced stress during N_2 characterization leads to structural deformation, these changes will be related to the structural rigidity of biochar. The nanostructure of biochar consists of small clusters of base structural units (BSU) consisting of stacks of graphene-like layers arranged close to parallel, and significant amounts of nonorganized graphene-like structures [20]. At temperatures around 400 °C, biochar consists mostly of amorphous carbon and short BSU clusters with significant amounts of heteroatoms, e.g. oxygen. These heteroatoms stabilize the carbon structure via enhancement of long-range interactions and provide structural flexibility by absorbing external stress through elastic interactions. Increasing the HTT to 700 °C leads to a partial release of heteroatoms, while the structural organization is still heteroatom-dominated, but the long-range stabilization is reduced [20, 80]. Since the structural organization in larger graphene sheets is not fully developed, the material exhibits low structural rigidity, increased mobility of the BSU units and an inability to distribute

externally induced stress among the solid matrix [81]. With a further increase of the HTT, the length of the graphene sheets increases and a BSU crosslink-dominated structure with long-range organization starts to develop [20]. The larger cross-linked BSU units at HTT 900 °C restrict the flexibility of the carbon matrix and impede structural deformation through external stress. These nanostructural arrangements are confirmed by the mechanical properties of biochar, indicating increasing hardness from 500 °C to 700 °C and a progressing lack of elastic interaction [81] as well as drop in the crushing strength around 600 °C [82, 83].

For samples suspected to display high elasticity, i.e. RH400 N_2 adsorption displays no open hysteresis, and no relevant changes could be observed in sequential CO_2 / N_2 measurements. With increasing HTT to 500 °C, the open hysteresis becomes more pronounced, although the absolute value of adsorption is still low. For RH700, the material is assumed to reach its maximum hardness, and the material becomes susceptible to swelling. The lack of elastic interaction inhibits a complete return to the original arrangement, and the material is partially deformed as seen in the diverting micropore volumes in sequential measurements. For RH900, the structural rigidity prevents excessive swelling, and the measured N_2 adsorption and open hysteresis show a consistent trend from RH400 < RH500 < RH900, in line with the CO_2 measurements. While structural changes were still detected in repeated CO_2-N_2 measurements, the magnitude was lower than for RH700. The changes in structural rearrangement and mechanical properties of biochar with increasing HTT and the effect of these structural changes on N_2 induced swelling can therefore provide an alternative explanation for the regularly observed micropore peak for biochars produced at 700 °C.

3.8 Hypothesis of a micropore structure collapse

The most common explanation for the continuous increase in SSA with increasing HTT before the SSA starts to decrease at higher temperature, is the theory of micropore collapse at

HTTs above 700 °C [12, 60, 64-67]. Similar to biochars from this study (Figure 9, left), several authors reported a characteristic Gaussian-shaped trend of SSA and pore volumes measured by N_2, which seems to confirm a structure collapse around 700 °C. However, it is essential to note that the origin of the micropore collapse theory is based on studies of activated carbon produced in oxidizing atmospheres which typically do not exhibit open hysteresis [55, 84].

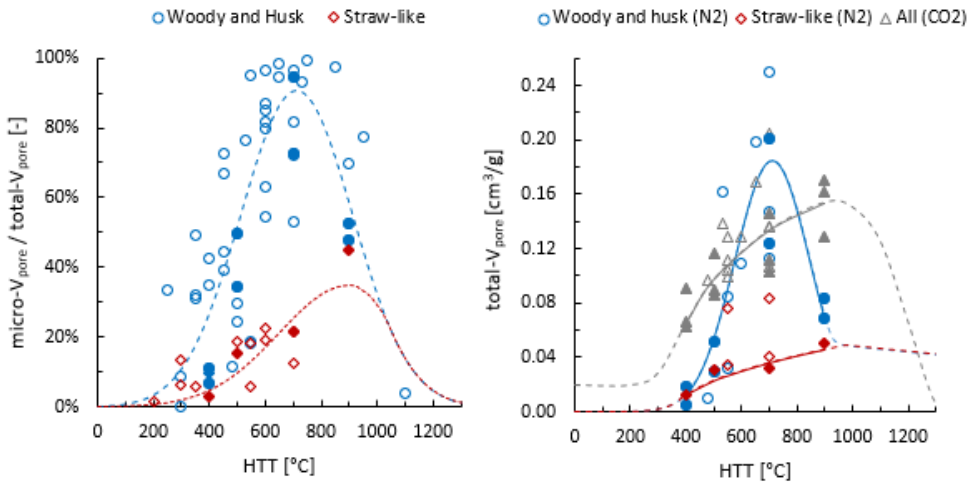

***Figure 9: Left** - Change of the micropore volume (N_2) / total pore volume (N_2) ratio plotted against HTT; data from this study and external data [18, 54-62]. **Right -** Change in the total pore volume (N_2, CO_2) with HTT; data from this study and external data [18, 54], (filled – this study, unfilled – external, solid line – data's regression line, dashed line - proposed extrapolation of trends; HTT – highest treatment temperature).*

Based on the observations from this study, we hypothesize that the characteristic peak in SSA and V_{pore} is at least partly based on adsorption induced pore deformation rather than micropore collapse. To test our hypothesis, we divided our whole dataset according to the feedstock source into wood-husk and straw-like derived biochars and compared the pore volume trends for samples with available N_2 and CO_2 data. As seen in Figure 9 (right), the pattern for total adsorption volumes measured by CO_2 resembles the N_2 pore volume trend for WS biochars. On the contrary, biochars produced from wood and husk biomass show significant deviations between 500 °C and 800 °C. Noticeable, the subset with available CO_2 data fits well into the broader dataset with N_2 measurements and shows similar trends for

wood/husk and straw biochars (Figure 9 (left), Table S2, S3, S6). This raises the question, why straw derived biochars behave differently. Similar to oxygen, other heteroatoms have the ability to stabilize the carbon structure by increasing the mobility of the BSU units and therefore, the structural resilience against external stress [20]. While the main heteroatom of wheat straw is silicon, a dominant influence of silicon is unlikely as rice husk with comparable levels of silicon shows a completely different trend. As observed in other studies, chlorine could be more relevant considering that straw biomass contains significant amounts of chlorine and is known to create conjugated cross-links between BSU units of the carbon matrix [20, 85]. The maximum release of chlorine occurs around 700 °C, which also coincides with growth in the measured microporosity of wheat straw [86, 87]. However, without detailed investigations into the effects of heteroatoms on the swelling ability of the carbon matrix, no definite conclusion can be made. It has to be highlighted that almost all studies reporting a micropore collapse at HTT close to 700°C are based on N_2 adsorption alone and do not use additional adsorbates such as CO_2. Considering the higher reliability of the micropore volume assessed by CO_2 [18, 31], a general micropore structure collapse cannot be identified from experimental data in this study. Besides the contradiction of a micropore collapse by CO_2 measurements, small-angle X-ray scattering analysis also contradicts a micropore collapse at HTTs below 1000 °C [88, 89]. The characteristic peak for biochar is therefore rather linked to N_2 measurement itself than the actual surface area and pore volume of the material.

3.9 Modified SSA calculation

As highlighted in this study, standard physisorption analysis of biochar using N_2 presents difficulties due to the presence of micropores as well as differing structural parameters which influence the results. To overcome these shortcomings, Jaggiello et al. [34] proposed a combined characterization of biochar using CO_2 and N_2 adsorption. However, due to limited analytical availability and therefore low adaption of standard CO_2 analysis, we propose an

adapted calculation based solely on N_2 adsorption with the use of the HS-NLDFT model as an alternative method [18]. By excluding the often-erroneous low-pressure region of N_2 isotherms, we argue that a more realistic SSA and V_{pore} for biochars can be obtained compared to the conventional BET method. Besides the observed difficulties in achieving correct low-pressure N_2 isotherms, pore sizes below 1.47 nm might also be of less significance for most biochar applications than accurate calculations of the large micropore and mesopore range. As most modern instruments have an automatic calculation of a variety of DFT kernels included, this would not increase the workload of researchers and can easily be implemented. Our proposed adaption of the DFT model is calculated by simply subtracting pores smaller than 1.47 nm from the cumulative surface area and pore volume.

The adjustment of the applied pore size range removes the peak at HTT 700 °C for wood and husk (W-H) derived chars. Straw-like (S-L) biochars are less influenced, which is in line with the suspected swelling behaviour seen for WD and RH and a better resembling of the combined assessment of CO_2 and N_2 (Figure S10 and Table S7). In Figure 10 and Table S8, the adjusted DFT model is compared to the conventional calculation on the whole dataset. Notably, the SSA of the adjusted model decreases considerably, while the peak at 700 °C seems almost completely removed, and a plateau-like development of the SSA displayed. We argue that this SSA evolution is a more realistic display of the trends indicated from structural models. The obtained comparison between the standard method and the adjusted model comprises important implications for engineering biochars with an optimised SSA. As the maximum of the SSA is shifted to lower temperatures around 500 °C, optimization studies relying on the

standard model might exhibit a misplaced optimum for SSA development [90]. Therefore, the proposed method can enable further advancements in biochar engineering.

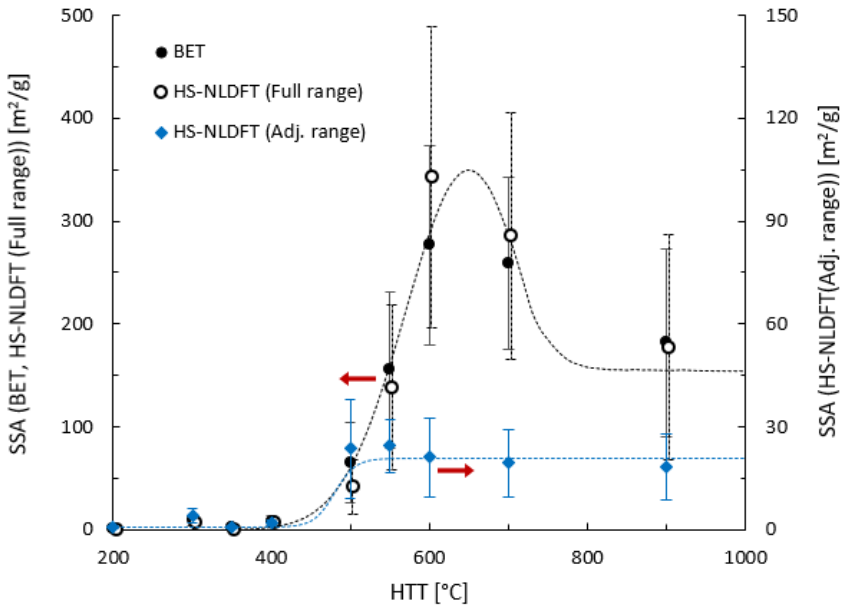

Figure. 10: *Changes of SSA (BET) and SSA (HS-NLDFT) with HTT for the combined dataset from this study and external data [18, 54-62] (n = 62), HS-NLDFT: full range - < 0.7 nm; adjusted range - < 1.47 nm).*

Along with the proposed adjusted calculation method, the need for standardization of N_2 physisorption measurements is evident. As suggested by Sigmund et al. [18], degassing temperatures should not be excessive. Besides an obligatory reporting of the measurement parameters, we recommend using an initial p/p_0 of 10^{-3} to avoid prolonged measurement times and excessive repetitive dosing during the measurement. If relevant microporosity is detected or the target pore size lies in the narrow micropore range for the material under consideration, the proposed adjusted SSA calculation for N_2 measurements should be accompanied by separate CO_2 characterisation to provide information about narrow micropores as shown by Diéguez-Alonso et al. [91].

4. Conclusions

In this study, we presented common obstacles for reliable surface area measurements of biochars. Biochar specific issues such as difficulties in correct parameter setting and long equilibrium times can lead to unreliable results and aggravate comparability between literature values. We show that the dominant influence of micropores on the surface area of biochar is further exaggerated by the measurement with N_2 and impacted by the structural rigidity of the material. Since micropores have a dominant influence on the SSA of biochars, this finding is significant for a better understanding of the SSA evolution of biochar related to the HTT. Based on our results, we propose an adapted SSA calculation which provides a more realistic representation of biochars' pore structure and enhances comparability of SSA assessments between biochars exhibiting different structural characteristics. Future research should focus on a direct determination of swelling using in-situ dilatometry as already done for other carbon materials and should be cross-validated by X-ray diffraction. Due to the diversity of biochar materials, systematic studies on the rigidity of the carbon matrix in relation to the production temperature would benefit our understanding of biomass pyrolysis and the evolution of derived parameters. The findings and recommendations in this paper should pave a path to a more accurate and reliable determination and reporting of biochar surface areas and porosity, which is key for optimization of biochar's performance in a wide range of applications and ultimately the ability to engineer specific biochar and biochar products tuned to the needs of target applications.

Declaration of competing interest

The authors declare no competing financial interests or personal relationships that could have appeared to influence the work reported in this paper.

CRediT authorship contribution statement

Przemyslaw Maziarka – Conceptualization, Investigation, Methodology, Formal analysis, Visualization, Writing - Original Draft, **Christian Wurzer** – Conceptualization, Investigation, Methodology, Formal analysis, Resources, Writing - Original Draft, **Pablo J. Arauzo** – Investigation, Resources, Writing - Review & Editing, **Alba Dieguez- Alonso** – Writing - Review & Editing, **Ondřej Mašek** – Funding acquisition, Writing - Review & Editing, **Frederik Ronsse** – Funding acquisition, Writing - Review & Editing

Acknowledgements

The authors would like to thank Prof. Andrea Kruse for granting access to the facilities at the University of Hohenheim, all researchers who provided raw data used in this study, and the anonymous reviewers for their valuable comments. Funding: This project received funding from the European Union's Horizon 2020 research and innovation programme under the Marie Skłodowska-Curie grant agreement No 721991.

References

[1] H. de Coninck, A. Revi, M. Babiker, P. Bertoldi, M. Buckeridge, A. Cartwright et al., Strengthening and Implementing the Global Response. In: Global Warming of 1.5°C. An IPCC Special Report on the impacts of global warming of 1.5°C above pre-industrial levels and related global greenhouse gas emission pathways, in the context of strengthening the global response to the threat of climate change, sustainable development, and efforts to eradicate poverty, in: V. MassonDelmotte, P. Zhai, H.-O. Pörtner, D. Roberts, J. Skea, P.R. Shukla et al. (Ed.), IPCC - The Intergovernmental Panel on Climate Change 2018, pp. 313 - 443.

[2] S.P. Sohi, E. Krull, E. Lopez-Capel, R. Bol, Chapter 2 - A Review of Biochar and Its Use and Function in Soil, Advances in Agronomy, Academic Press2010, pp. 47-82.

[3] L. Zhao, X. Cao, O. Mašek, A. Zimmerman, Heterogeneity of biochar properties as a function of feedstock sources and production temperatures, Journal of Hazardous Materials 256-257 (2013) 1-9.

[4] W.-J. Liu, H. Jiang, H.-Q. Yu, Development of Biochar-Based Functional Materials: Toward a Sustainable Platform Carbon Material, Chemical Reviews 115 (22) (2015) 12251-12285.

[5] B. Kavitha, P.V.L. Reddy, B. Kim, S.S. Lee, S.K. Pandey, K.-H. Kim, Benefits and limitations of biochar amendment in agricultural soils: A review, Journal of Environmental Management 227 (2018) 146-154.

[6] L. Wang, Y.S. Ok, D.C.W. Tsang, D.S. Alessi, J. Rinklebe, H. Wang et al., New trends in biochar pyrolysis and modification strategies: feedstock, pyrolysis conditions, sustainability concerns and implications for soil amendment, Soil Use and Management 36(3) (2020) 358-386.

[7] D. Mohan, A. Sarswat, Y.S. Ok, C.U. Pittman, Organic and inorganic contaminants removal from water with biochar, a renewable, low cost and sustainable adsorbent – A critical review, Bioresource Technology 160 (2014) 191-202.

[8] L. Ye, Z. Peng, L. Wang, A. Anzulevich, I. Bychkov, D. Kalganov et al., Use of Biochar for Sustainable Ferrous Metallurgy, JOM 71(11) (2019) 3931-3940.

[9] R.S. Gabhi, D.W. Kirk, C.Q. Jia, Preliminary investigation of electrical conductivity of monolithic biochar, Carbon 116 (2017) 435-442.

[10] P. Thomas, C.W. Lai, M.R. Bin Johan, Recent developments in biomass-derived carbon as a potential sustainable material for super-capacitor-based energy storage and environmental applications, Journal of Analytical and Applied Pyrolysis 140 (2019) 54-85.

[11] V.L. Morales, F.J. Pérez-Reche, S.M. Hapca, K.L. Hanley, J. Lehmann, W. Zhang, Reverse engineering of biochar, Bioresource Technology 183 (2015) 163-174.

[12] A. Dieguez-Alonso, A. Funke, A. Anca-Couce, A.G. Rombolà, G. Ojeda, J. Bachmann et al., Towards biochar and hydrochar engineering—influence of process conditions on surface physical and chemical properties, thermal stability, nutrient availability, toxicity and wettability, Energies 11(3) (2018) 496.

[13] S. Weldon, D.P. Rasse, A. Budai, O. Tomic, P. Dörsch, The effect of a biochar temperature series on denitrification: which biochar properties matter?, Soil Biology and Biochemistry 135 (2019) 173-183.

[14] F. Ronsse, S. van Hecke, D. Dickinson, W. Prins, Production and characterization of slow pyrolysis biochar: influence of feedstock type and pyrolysis conditions, GCB Bioenergy 5(2) (2013) 104-115.

[15] W.-J. Liu, W.-W. Li, H. Jiang, H.-Q. Yu, Fates of Chemical Elements in Biomass during Its Pyrolysis, Chemical Reviews 117(9) (2017) 6367-6398.

[16] K. Crombie, O. Mašek, S.P. Sohi, P. Brownsort, A. Cross, The effect of pyrolysis conditions on biochar stability as determined by three methods, GCB Bioenergy 5(2) (2013) 122-131.

[17] A.D. Igalavithana, S. Mandal, N.K. Niazi, M. Vithanage, S.J. Parikh, F.N.D. Mukome et al., Advances and future directions of biochar characterization methods and applications, Critical Reviews in Environmental Science and Technology 47(23) (2017) 2275-2330.

[18] G. Sigmund, T. Hüffer, T. Hofmann, M. Kah, Biochar total surface area and total pore volume determined by N2 and CO2 physisorption are strongly influenced by degassing temperature, Science of The Total Environment 580 (2017) 770-775.

[19] B. Singh, M.C. Arbestain, J. Lehmann, Biochar : analytical methods - a practical guide, 2017.

[20] J.S. McDonald-Wharry, M. Manley-Harris, K.L. Pickering, Reviewing, Combining, and Updating the Models for the Nanostructure of Non-Graphitizing Carbons Produced from Oxygen-Containing Precursors, Energy & Fuels 30(10) (2016) 7811-7826.

[21] M. Keiluweit, P.S. Nico, M.G. Johnson, M. Kleber, Dynamic Molecular Structure of Plant Biomass-Derived Black Carbon (Biochar), Environmental Science & Technology 44(4) (2010) 1247-1253.

[22] A.K. Kercher, D.C. Nagle, Microstructural evolution during charcoal carbonization by X-ray diffraction analysis, Carbon 41(1) (2003) 15-27.

[23] P.J. Arauzo, P.A. Maziarka, M.P. Olszewski, R.L. Isemin, N.S. Muratova, F. Ronsse et al., Valorization of the poultry litter through wet torrefaction and different activation treatments, Science of The Total Environment 732 (2020) 139288.

[24] J.E. Aguiar, J.C.A. de Oliveira, P.F.G. Silvino, J.A. Neto, I.J. Silva, S.M.P. Lucena, Correlation between PSD and adsorption of anionic dyes with different molecular weigths on activated carbon, Colloids and Surfaces A: Physicochemical and Engineering Aspects 496 (2016) 125-131.

[25] C. Pelekani, V.L. Snoeyink, Competitive adsorption between atrazine and methylene blue on activated carbon: the importance of pore size distribution, Carbon 38(10) (2000) 1423-1436.

[26] W. Hao, E. Björkman, M. Lilliestråle, N. Hedin, Activated carbons prepared from hydrothermally carbonized waste biomass used as adsorbents for CO2, Applied Energy 112 (2013) 526-532.

[27] A.M. Dehkhoda, E. Gyenge, N. Ellis, A novel method to tailor the porous structure of KOH-activated biochar and its application in capacitive deionization and energy storage, Biomass and Bioenergy 87 (2016) 107-121.

[28] S. Li, J. Lu, T. Zhang, Y. Cao, J. Li, Relationship between biochars' porosity and adsorption of three neutral herbicides from water, Water Sci Technol 75(2) (2017) 482-489.

[29] A. Budai, L. Wang, M. Gronli, L.T. Strand, M.J. Antal, S. Abiven et al., Surface Properties and Chemical Composition of Corncob and Miscanthus Biochars: Effects of Production Temperature and Method, Journal of Agricultural and Food Chemistry 62(17) (2014) 3791-3799.

[30] K.A. Cychosz, M. Thommes, Progress in the Physisorption Characterization of Nanoporous Gas Storage Materials, Engineering 4(4) (2018) 559-566.

[31] K.T. Klasson, M. Uchimiya, I.M. Lima, Characterization of narrow micropores in almond shell biochars by nitrogen, carbon dioxide, and hydrogen adsorption, Industrial Crops and Products 67 (2015) 33-40.

[32] S. Lowell, J.E. Shields, M.A. Thomas, Characterization of porous solids and powders surface area, pore size and density, Springer, Dordrecht, 2011.

[33] F. Rouquerol, Adsorption by Powders and Porous Solids : principles, methodology and applications, Academic press, Oxford, 2014.

[34] J. Jagiello, C. Ania, J.B. Parra, C. Cook, Dual gas analysis of microporous carbons using 2D-NLDFT heterogeneous surface model and combined adsorption data of N2 and CO2, Carbon 91 (2015) 330-337.

[35] M. Thommes, K. Kaneko, V. Neimark Alexander, P. Olivier James, F. Rodriguez-Reinoso, J. Rouquerol et al., Physisorption of gases, with special reference to the evaluation of surface area and pore size distribution (IUPAC Technical Report), Pure and Applied Chemistry, 2015, p. 1051.

[36] P. Baran, K. Zarębska, M. Bukowska, Expansion of Hard Coal Accompanying the Sorption of Methane and Carbon Dioxide in Isothermal and Non-isothermal Processes, Energy & Fuels 29(3) (2015) 1899-1904.

[37] S. Day, R. Fry, R. Sakurovs, Swelling of moist coal in carbon dioxide and methane, International Journal of Coal Geology 86(2) (2011) 197-203.

[38] K. Czerw, P. Baran, K. Zarębska, Application of the stretched exponential equation to sorption of mine gases and sorption induced swelling of bituminous coal, International Journal of Coal Geology 173 (2017) 76-83.

[39] P. Kowalczyk, A. Ciach, A.V. Neimark, Adsorption-Induced Deformation of Microporous Carbons: Pore Size Distribution Effect, Langmuir 24(13) (2008) 6603-6608.

[40] C. Balzer, R.T. Cimino, G.Y. Gor, A.V. Neimark, G. Reichenauer, Deformation of Microporous Carbons during N2, Ar, and CO2 Adsorption: Insight from the Density Functional Theory, Langmuir 32(32) (2016) 8265-8274.

[41] K.E. Hart, J.M. Springmeier, N.B. McKeown, C.M. Colina, Simulated swelling during low-temperature N2 adsorption in polymers of intrinsic microporosity, Physical Chemistry Chemical Physics 15(46) (2013) 20161-20169.

[42] A.V. Neimark, F.-X. Coudert, A. Boutin, A.H. Fuchs, Stress-Based Model for the Breathing of Metal−Organic Frameworks, The Journal of Physical Chemistry Letters 1(1) (2010) 445-449.

[43] W.J. Braida, J.J. Pignatello, Y. Lu, P.I. Ravikovitch, A.V. Neimark, B. Xing, Sorption Hysteresis of Benzene in Charcoal Particles, Environmental Science & Technology 37(2) (2003) 409-417.

[44] EBC, "European Biochar Certificate - Guidelines for a Sustainable Production of Biochar." European Biochar Foundation (EBC), Arbaz, Switzerland, (https://European-biochar.org), Version 9.0E of 1st June 2020.

[45] K.S.W. Sing, Characterization of porous materials: past, present and future, Colloids and Surfaces A: Physicochemical and Engineering Aspects 241(1) (2004) 3-7.

[46] S. Brunauer, P.H. Emmett, E. Teller, Adsorption of Gases in Multimolecular Layers, Journal of the American Chemical Society 60(2) (1938) 309-319.

[47] J. Rouquerol, P. Llewellyn, F. Rouquerol, Is the bet equation applicable to microporous adsorbents?, in: P.L. Llewellyn, F. Rodriquez-Reinoso, J. Rouqerol, N. Seaton (Eds.), Studies in Surface Science and Catalysis, Elsevier, 2007, pp. 49-56.

[48] B. Janković, N. Manić, V. Dodevski, I. Radović, M. Pijović, Đ. Katnić et al., Physico-chemical characterization of carbonized apricot kernel shell as precursor for activated carbon preparation in clean technology utilization, Journal of Cleaner Production 236 (2019) 117614.

[49] J. Landers, G.Y. Gor, A.V. Neimark, Density functional theory methods for characterization of porous materials, Colloids and Surfaces A: Physicochemical and Engineering Aspects 437 (2013) 3-32.

[50] A.M. Puziy, O.I. Poddubnaya, B. Gawdzik, M. Sobiesiak, Comparison of heterogeneous pore models QSDFT and 2D-NLDFT and computer programs ASiQwin and SAIEUS for calculation of pore size distribution, Adsorption 22(4) (2016) 459-464.

[51] H.J. Bachmann, T.D. Bucheli, A. Dieguez-Alonso, D. Fabbri, H. Knicker, H.-P. Schmidt et al., Toward the Standardization of Biochar Analysis: The COST Action TD1107 Interlaboratory Comparison, Journal of Agricultural and Food Chemistry 64(2) (2016) 513-527.

[52] M. Thommes, K.A. Cychosz, Physical adsorption characterization of nanoporous materials: progress and challenges, Adsorption 20(2) (2014) 233-250.

[53] O. Mašek, W. Buss, A. Roy-Poirier, W. Lowe, C. Peters, P. Brownsort et al., Consistency of biochar properties over time and production scales: A characterisation of standard materials, Journal of Analytical and Applied Pyrolysis 132 (2018) 200-210.

[54] V. Gargiulo, A. Gomis-Berenguer, P. Giudicianni, C.O. Ania, R. Ragucci, M. Alfè, Assessing the Potential of Biochars Prepared by Steam-Assisted Slow Pyrolysis for CO2 Adsorption and Separation, Energy & Fuels 32(10) (2018) 10218-10227.

[55] H. Yang, B. Huan, Y. Chen, Y. Gao, J. Li, H. Chen, Biomass-Based Pyrolytic Polygeneration System for Bamboo Industry Waste: Evolution of the Char Structure and the Pyrolysis Mechanism, Energy & Fuels 30(8) (2016) 6430-6439.

[56] Z. Wang, H. Zheng, Y. Luo, X. Deng, S. Herbert, B. Xing, Characterization and influence of biochars on nitrous oxide emission from agricultural soil, Environmental Pollution 174 (2013) 289-296.

[57] S. Yu, J. Park, M. Kim, C. Ryu, J. Park, Characterization of biochar and byproducts from slow pyrolysis of hinoki cypress, Bioresource Technology Reports 6 (2019) 217-222.

[58] J. Zhang, X. Hu, K. Zhang, Y. Xue, Desorption of calcium-rich crayfish shell biochar for the removal of lead from aqueous solutions, Journal of Colloid and Interface Science 554 (2019) 417-423.

[59] A. Reyhanitabar, E. Frahadi, H. Ramezanzadeh, S. Oustan, Effect of Pyrolysis Temperature and Feedstock Sources on Physicochemical Characteristics of Biochar, mdrsjrns 22(2) (2020) 547-561.

[60] B. Ji, L. Zhu, H. Song, W. Chen, S. Guo, F. Chen, Adsorption of Methylene Blue onto Novel Biochars Prepared from Magnolia grandiflora Linn Fallen Leaves at Three Pyrolysis Temperatures, Water, Air, & Soil Pollution 230(12) (2019) 281.

[61] A. Ayala-Cortés, C.A. Arancibia-Bulnes, H.I. Villafán-Vidales, D.R. Lobato-Peralta, D.C. Martínez-Casillas, A.K. Cuentas-Gallegos, Solar pyrolysis of agave and tomato pruning wastes: Insights of the effect of pyrolysis operation parameters on the physicochemical properties of biochar, AIP Conference Proceedings 2126(1) (2019) 180001.

[62] D. Fuentes-Cano, L. von Berg, A. Diéguez-Alonso, R. Scharler, A. Gómez-Barea, A. Anca-Couce, Tar conversion of biomass syngas in a downstream char bed, Fuel Processing Technology 199 (2020) 106271.

[63] T.A. Centeno, F. Stoeckli, The assessment of surface areas in porous carbons by two model-independent techniques, the DR equation and DFT, Carbon 48(9) (2010) 2478-2486.

[64] S. Yoo, S.S. Kelley, D.C. Tilotta, S. Park, Structural Characterization of Loblolly Pine Derived Biochar by X-ray Diffraction and Electron Energy Loss Spectroscopy, ACS Sustainable Chemistry & Engineering 6(2) (2018) 2621-2629.

[65] G. Yang, Z. Wang, Q. Xian, F. Shen, C. Sun, Y. Zhang et al., Effects of pyrolysis temperature on the physicochemical properties of biochar derived from vermicompost and its potential use as an environmental amendment, RSC Advances 5(50) (2015) 40117-40125.

[66] Y. Chen, X. Zhang, W. Chen, H. Yang, H. Chen, The structure evolution of biochar from biomass pyrolysis and its correlation with gas pollutant adsorption performance, Bioresource Technology 246 (2017) 101-109.

[67] R.A. Brown, A.K. Kercher, T.H. Nguyen, D.C. Nagle, W.P. Ball, Production and characterization of synthetic wood chars for use as surrogates for natural sorbents, Organic Geochemistry 37(3) (2006) 321-333.

[68] W. Lai, S. Yang, Y. Jiang, F. Zhao, Z. Li, B. Zaman et al., Artefact peaks of pore size distributions caused by unclosed sorption isotherm and tensile strength effect, Adsorption 26(4) (2020) 633-644.

[69] J. Jagiello, J. Kenvin, A. Celzard, V. Fierro, Enhanced resolution of ultra micropore size determination of biochars and activated carbons by dual gas analysis using N_2 and CO_2 with 2D-NLDFT adsorption models, Carbon 144 (2019) 206-215.

[70] Quantachrome Instruments - I03IA003EN-A - Obtaining High Resolution, Low Pressure Isotherms with a Constant Volume/VectorDoseTM Method, POWDER TECH NOTE, p. 3.

[71] T.D. Bucheli, Ö. Gustafsson, Quantification of the Soot-Water Distribution Coefficient of PAHs Provides Mechanistic Basis for Enhanced Sorption Observations, Environmental Science & Technology 34(24) (2000) 5144-5151.

[72] M.T.O. Jonker, A.A. Koelmans, Extraction of Polycyclic Aromatic Hydrocarbons from Soot and Sediment: Solvent Evaluation and Implications for Sorption Mechanism, Environmental Science & Technology 36(19) (2002) 4107-4113.

[73] C.-M. Popescu, C.A.S. Hill, R. Anthony, G. Ormondroyd, S. Curling, Equilibrium and dynamic vapour water sorption properties of biochar derived from apple wood, Polymer Degradation and Stability 111 (2015) 263-268.

[74] M. Sander, J.J. Pignatello, On the Reversibility of Sorption to Black Carbon: Distinguishing True Hysteresis from Artificial Hysteresis Caused by Dilution of a Competing Adsorbate, Environmental Science & Technology 41(3) (2007) 843-849.

[75] V.V. Sizov, E.M. Piotrovskaya, E.N. Brodskaya, Influence of a Surface Microheterogeneity on the Disjoining Pressure of Adsorbed Lennard–Jones Fluid. Computer Simulation, Colloid Journal 65(6) (2003) 772-777.

[76] E.A. Ustinov, D.D. Do, Effect of adsorption deformation on thermodynamic characteristics of a fluid in slit pores at sub-critical conditions, Carbon 44(13) (2006) 2652-2663.

[77] A.V. Tvardovskiy, Sorbent deformation, Elsevier Academic Press, Amsterdam, 2007.

[78] P. Kowalczyk, C. Balzer, G. Reichenauer, A.P. Terzyk, P.A. Gauden, A.V. Neimark, Using in-situ adsorption dilatometry for assessment of micropore size distribution in monolithic carbons, Carbon 103 (2016) 263-272.

[79] R. Diao, C. Fan, D.D. Do, D. Nicholson, Monte Carlo Simulation of Adsorption-Induced Deformation in Finite Graphitic Slit Pores, The Journal of Physical Chemistry C 120(51) (2016) 29272-29282.

[80] D.B. Wiedemeier, S. Abiven, W.C. Hockaday, M. Keiluweit, M. Kleber, C.A. Masiello et al., Aromaticity and degree of aromatic condensation of char, Organic Geochemistry 78 (2015) 135-143.

[81] G.A. Zickler, T. Schöberl, O. Paris, Mechanical properties of pyrolysed wood: a nanoindentation study, Philosophical Magazine 86(10) (2006) 1373-1386.

[82] M. Kumar, B.B. Verma, R.C. Gupta, Mechanical Properties of Acacia and Eucalyptus Wood Chars, Energy Sources 21(8) (1999) 675-685.

[83] M. Kumar, S. Jena, Influence of Carbonization Conditions on the Properties of Coconut Shell Chars, Energy Sources, Part A: Recovery, Utilization, and Environmental Effects 28(5) (2006) 423-431.

[84] A. Paethanom, K. Yoshikawa, Influence of Pyrolysis Temperature on Rice Husk Char Characteristics and Its Tar Adsorption Capability, Energies 5(12) (2012) 4941-4951.

[85] S.V. Vassilev, D. Baxter, L.K. Andersen, C.G. Vassileva, An overview of the chemical composition of biomass, Fuel 89(5) (2010) 913-933.

[86] J.M. Johansen, J.G. Jakobsen, F.J. Frandsen, P. Glarborg, Release of K, Cl, and S during Pyrolysis and Combustion of High-Chlorine Biomass, Energy & Fuels 25(11) (2011) 4961-4971.

[87] B. Peng, X. Li, J. Luo, X. Yu, Fate of Chlorine in Rice Straw under Different Pyrolysis Temperatures, Energy & Fuels 33(9) (2019) 9272-9279.

[88] B. Smarsly, M. Antonietti, T. Wolff, Evaluation of the small-angle x-ray scattering of carbons using parametrization methods, The Journal of Chemical Physics 116(6) (2002) 2618-2627.

[89] M. Wiener, G. Reichenauer, Microstructure of porous carbons derived from phenolic resin – Impact of annealing at temperatures up to 2000°C analyzed by complementary characterization methods, Microporous and Mesoporous Materials 203 (2015) 116-122.

[90] S.C. Peterson, M.A. Jackson, S. Kim, D.E. Palmquist, Increasing biochar surface area: Optimization of ball milling parameters, Powder Technology 228 (2012) 115-120.

[91] A. Diéguez-Alonso, A. Anca-Couce, V. Frišták, E. Moreno-Jiménez, M. Bacher, T.D. Bucheli et al., Designing biochar properties through the blending of biomass feedstock with metals: Impact on oxyanions adsorption behavior, Chemosphere 214 (2019) 743-753.